Active Disturbance Rejection Control of Nuclear Pressurized Water Reactor for Power Generation

Ahmad, Saif; Abdulraheem, Kamal Kayode ; Tolokonsky, Andrei Olegovich ; Ahmed, Hafiz

2022 4th Global Power, Energy and Communication Conference (GPECOM)

DOI:
https://doi.org/10.1109/GPECOM55404.2022.9815709

Published: 11/07/2022

Peer reviewed version

Active Disturbance Rejection Control of Nuclear Pressurized Water Reactor for Power Generation

Saif Ahmad
Department of Electrical Engineering
Indian Institute of Technology Patna
Patna, India
E-mail: saifiitp16@gmail.com

Kamal Kayode Abdulraheem
Automation Department
National Nuclear Research University
Moscow Engineering Physics Institute (MEPHI) and
Nigeria Atomic Energy Commission
E-mail: kamalabdulraheem@gmail.com

Andrei Olegovich Tolokonsky
Automation Department
National Nuclear Research University
Moscow Engineering Physics Institute (MEPHI)
E-mail: toloconne@mail.ru

Hafiz Ahmed
Nuclear Futures Institute
Bangor University
Bangor LL57 1UT, United Kingdom
E-mail: hafiz.h.ahmed@ieee.org

***Abstract*—Control design for pressurized water reactor (PWR) is difficult due to associated non-linearity, modelling uncertainties and time-varying system parameters. Extended state observer (ESO) based active disturbance rejection control (ADRC) presents a simple and robust control solution which is almost model free and has few tuning parameters. However, conventional ESO suffers from noise over-amplification in the obtained estimates due to high-gain construction which in turn degrades the noise sensitivity of the closed-loop system and limits the achievable dynamic performance in practical scenarios. To overcome this problem, two recent techniques namely cascade ESO (CESO) and low-power higher-order ESO (LHESO) are implemented for control of PWR. Simulation analysis conducted in MATLAB illustrates the performance improvement obtained over conventional ESO based ADRC. Extensive simulation analysis is also conducted to investigate robustness towards parametric uncertainties.**

***Index Terms*—Pressurized water reactor, active disturbance rejection control, extended state observer, measurement noise.**

I. Introduction

The world is grappling with increasing demand for reliable, sustainable, and clean energy. There are several sources of energy including renewables, fossil fuels, and nuclear energy. Fossil fuels are responsible for the average rise in global temperature due to greenhouse gases, and they also cause pollution with concomitant effects on human health and the environment. Consequently, efforts to reduce pollution and global temperatures to avoid catastrophic events include the replacement of fossil fuels with clean energy sources. Renewable energy sources including solar, and wind energy have been identified as replacements for fossil fuels. However, they are incapable of providing bulk energy as fossil fuels. Instead, nuclear energy can be used as an adequate and effective substitute for fossil fuels. Technological advancements have enabled the application of nuclear power plants in the load-following mode, thereby making nuclear power plants operable as baseloads, or peak load plants. Nonetheless, safe and reliable application of nuclear energy requires efficient control systems to avoid accidents that can lead to fuel melting and the subsequent release of radioactive materials into the environment.

Researchers and practitioners have considered several control techniques for nuclear reactor core power control systems to improve the system performance and availability, including state feedback and optimal control techniques. A state feedback controller was designed based on a linear quadratic regulator (LQR) for a CANDU heavy water reactor control system [1]and an LQG/LTR technique to control a pressurized water reactor (PWR) [2]. A state feedback which uses a classical differential lag compensator assisted by LQG/LTR was used to control the core power of a PWR in [3]. To further enhance optimal state feedback control, an LQG, PID and an optimization Improved Adaptive Genetic Algorithm (IAGA) were combined to synthesize a new control paradigm for the core power control of a nuclear reactor [4]. Nonetheless, Optimal state feedback control performance degrades with time in an uncertain environment such as a nuclear reactor, and it is not robust against external disturbances [5]. In addition, none of the control paradigms considered external disturbances in their design. Thus, hybrid control techniques which combine LQG/LTR with sliding mode control [5], [6], and Linear Quadratic Integrator, Linear Quadratic Gaussian and Loop Transfer Recovery (LQGI/LTR) [7], were designed to improve the robustness of the optimal control techniques against external disturbances. On the other hand, advanced control techniques such as model predictive control [8], fuzzy logic control [9] and artificial neural network algorithm [10]

The work of H. Ahmed is funded through the Sêr Cymru II 80761-BU-103 project by Welsh European Funding Office (WEFO) under the European Regional Development Fund (ERDF)

978-1-6654-6925-8/22/$31.00 ©2022 IEEE

are computationally intensive and sensitive towards parametric perturbations. Robust techniques such as sliding mode control suffer from chattering problem [11], [12] which has recently been addressed in [13]–[15]. It should be noted that most of control schemes discussed thus far are based on passive disturbance attenuation or rejection approach. Thus, a new control paradigm that actively compensates disturbances in nuclear power plant control systems is required for system safety, efficiency, and reliability. Recently, several studies have used the active disturbance rejection control (ADRC) technique in nuclear reactor control loops owing to its effectiveness in dealing with system nonlinearities and modelling uncertainty as well as parametric variations. Besides, it is simple to implement and tune, and requires minimal plant information in terms of the relative degree and input gain [16]–[19]. However, most of the studies on ADRC do not consider the effect of measurement noise which is ubiquitous in practical systems and degrades the quality of estimates obtained via extended state observers (ESO) which in turn limits the achievable closed-loop performance. Motivated by the gap observed in this area, we apply two recently proposed noise suppressing ESOs namely low-power higher-order ESO (LHESO) [20] and cascade ESO (CESO) [21], [22] for control of PWR under the effect of non-negligible sensor noise. Through extensive simulation studies, we illustrate that the noise suppressing ESO based ADRC techniques offer improved resilience towards high-frequency measurement noise along with better closed loop performance in terms of reference tracking as well as disturbance attenuation. In addition to the nominal operating condition, eight different perturbed scenarios with positive as well as negative deviations of critical PWR parameters are considered to analyse the robustness of the developed schemes.

II. Modeling of Pressurized Water Reactor

Generally, the Boltzmann transport equation captures time-dependent flux distribution in a nuclear reactor. However, exact solutions of the equation can be obtained for a few rare scenarios. Nevertheless, the approximate neutron diffusion equation where the energy variable is discretized and intergroup transfer cross sections represent the slowing-down process can adequately be used instead of the transport equation [23]. In addition, the control system design requires simple systems of first-order differential equations. Therefore, the neutron diffusion equation, including delayed neutrons, was used for the derivation of the reactor Point kinetics equation, which is a set of first-order equations. The point kinetics equation is a fundamental equation that describes the time-dependence of reactor core multiplication. It can be used to predict the behavior of the neutron population in a reactor [24]. The detailed derivation of the equation is given by [24], [25].

The Point kinetics model, which accounts for the neutronic model is coupled with other models including the thermal-hydraulics and reactivity models. The thermal-hydraulics model account for the temperature reactivity feedback owing to the doppler effect and coolant. The thermal-hydraulic model is based on a singly lumped model of the fuel and coolant temperatures. Lastly, the reactivity model accounts for the total reactivity including the external reactivity of the control rods. Therefore, the model comprises three main parts: the neutronic model, thermal-hydraulics model, and reactivity model. Therefore, the reactivity model comprises the reactivity owing to control rod, the coolant, and fuel temperature. The complete model for the nuclear reactor is therefore given as follows:

$$\begin{aligned}
\dot{n}_r &= (\rho-\beta)\Lambda^{-1}n_r + \beta\Lambda^{-1}c_r \\
\dot{c}_r &= \lambda(n_r - c_r) \\
\dot{T}_f &= \mu_f^{-1}\big[f_f P_0 n_r - \Omega T_f + 0.5\Omega(T_l + T_e)\big] \\
\dot{T}_l &= \mu_c^{-1}\big[(1-f_f)P_0 n_r + \Omega T_f - (M+0.5\Omega)T_l \\
&\qquad + (M-0.5\Omega)T_e\big] \\
\dot{\rho}_r &= G_r z_r \\
\rho &= \rho_r + \alpha_f(T_f - T_{f0}) + 0.5\alpha_c(T_l - T_{l0}) \\
&\qquad + 0.5\alpha_c(T_e - T_{e0}),
\end{aligned} \tag{1}$$

where $P = P_0 n_r$ is the power output and $\alpha_f(n_r) = (n_r - 4.24) \times 10^{-5}\frac{\delta k}{k}/^\circ C, \alpha_c(n_r) = -(4n_r + 17.3) \times 10^{-5}\frac{\delta k}{k}/^\circ C, \mu_c(n_r) = \frac{160}{9}n_r + 54.022\ MW\cdot s/^\circ C, \Omega(n_r) = \frac{5}{3}n_r + 4.933\ MW\cdot s/^\circ C,\ M(n_r) = (28n_r + 74) MW\cdot s/^\circ C$ are the coefficients. Nomenclature used for the modelling the PWR is given in Table I.

TABLE I: Nomenclature.

n_r	- Neutron density relative to initial equilibrium point
n_{r0}	- Initial equilibrium neutron density
c	- Precursor density
c_0	- Equilibrium precursor density at rated power
λ	- Effective precursor radioactive decay constant
ρ	- Total reactivity
ρ_r	- Reactivity induced by the control mechanism
Λ	- Effective prompt neutron life time
β	- Total delayed neutron fraction
T_e	- Temperature of water entering the reactor
z_r	- Control input, control rod speed in units of fraction of core length per second
G_r	- Total reactivity of control rod
α_f	- Fuel temperature reactivity coefficient
α_c	- Coolant temperature reactivity coefficient
T_f	- Average reactor fuel temperature
T_{f0}	- Initial equilibrium average reactor fuel temperature
T_l	- Temperature of water leaving the reactor
T_{l0}	- Initial equilibrium (steady state) temperature of water leaving the reactor
μ_f	- Total heat capacity of fuel
μ_c	- Total heat capacity of reactor coolant
Ω	- Heat transfer coefficient between fuel and coolant
M	- Mass flow rate multiplied by heat capacity of coolant
f_f	- Fraction of reactor power deposited in the fuel
P_0	- Rated Thermal power

III. Active Disturbance Rejection Control (ADRC)

Dynamic model of a PWR expressed in (1) is highly nonlinear and has time-varying parameters. Furthermore, using the entire higher-order system dynamics may lead to

a complex control structure that is difficult to design and implement. Active disturbance rejection control (ADRC) [26], [27] presents a simple and intuitive solution to this problem by considering the nominal model as a cascaded chain of integrators where the system order relies on the relative degree of the actual system and only approximate information about the input gain of the system is required. In doing so, ADRC expands the notion of disturbance by considering only the required minimal system information for controller design and categorising any deviation from the assumed nominal model as total disturbance.

Rewriting the neutron dynamics as

$$\frac{dn_r}{dt} = -\frac{\beta}{\Lambda}\big(n_r - c_r\big) + \frac{n_r}{\Lambda}\Big[\int_0^t G_r z_r d\tau + \alpha_f \Delta T_f + 0.5\alpha_c\big(\Delta T_l + \Delta T_e\big)\Big], \tag{2}$$

using (1), it can be observed that the relative degree of the PWR dynamics is two as the control input z_r appears in the second derivative of the preceding neutron dynamics. It is therefore possible to rewrite the 5^{th} order dynamics of PWR using a second order integral chain form given by

$$\ddot{n}_r = b_0 z_r + f \tag{3}$$

where $b_0(n_r) = G_r n_r/\Lambda$ is the input gain and f is the total disturbance expressed as$f = \frac{G_r(n_r - n_{r0})}{\Lambda} z_r + \frac{n_r}{\Lambda}[\dot{\alpha}_f \Delta T_f + \alpha_f \Delta \dot{T}_f + 0.5\dot{\alpha}_c(\Delta T_l + \Delta T_e) + 0.5\alpha_c(\Delta \dot{T}_l + \Delta \dot{T}_e)] - \frac{\beta}{\Lambda}\big(\dot{n}_r - \dot{c}_r\big) + \frac{\dot{n}_r}{\Lambda}\Big[\int_0^t G_r z_r d\tau + \alpha_f \Delta T_f + 0.5\alpha_c\big(\Delta T_l + \Delta T_e\big)\Big]$. Considering the total disturbance f as a virtual state variable (x_3) that needs to be estimated along with the system states (x_1, x_2), the augmented state-space model is expressed as

$$\begin{aligned} \dot{x}_1 &= x_2 \\ \dot{x}_2 &= x_3 + b_0 u \\ \dot{x}_3 &= h \\ y &= x_1 + \nu \end{aligned} \tag{4}$$

where $x_1 = n_r$ is the output to be controlled, $u = z_r$ is the control input, $h = \dot{f}$ and ν denotes the effect of measurement noise. The compact matrix form for (4) is given by

$$\begin{aligned} \dot{\boldsymbol{x}} &= \boldsymbol{\mathcal{A}}\boldsymbol{x} + b_0\boldsymbol{\mathcal{B}}u + \boldsymbol{E}h \\ y &= \boldsymbol{C}\boldsymbol{x} + \nu, \end{aligned} \tag{5}$$

where $\boldsymbol{x} = [x_1,\ x_2,\ x_3]^T$ and the associated matrices are defined as $\boldsymbol{\mathcal{A}} = \begin{bmatrix} \boldsymbol{0} & \boldsymbol{I}_2 \\ 0 & \boldsymbol{0} \end{bmatrix}_{3\times 3}$, $\boldsymbol{\mathcal{B}} = \begin{bmatrix} 0 & 1 & 0 \end{bmatrix}^T_{1\times 3}$, $\boldsymbol{C} = \begin{bmatrix} 1 & \boldsymbol{0} \end{bmatrix}_{1\times 3}$, $\boldsymbol{E} = \begin{bmatrix} \boldsymbol{0} & 1 \end{bmatrix}^T_{1\times 3}$.

Assuming that the state as well as disturbance estimates are available, a disturbance decoupling control law of the form

$$u = b_0^{-1}\big[-\hat{x}_3 + \bar{u}\big], \tag{6}$$

can be implemented to reduce the perturbed nominal model to a pure integrating form, while a stabilizing nominal controller can be selected as

$$\bar{u} = k_1(r - \hat{x}_1) - k_2\hat{x}_2 \tag{7}$$

to obtain desired closed-loop dynamics. The required estimates of $x_i,\ i = \{1, 2, 3\}$ are obtained via an extended state observer (ESO) designed for the augmented state-space model expressed in (5). As highlighted in [20]–[22], [28], conventional ESO suffers from noise amplification problem in the obtained estimates due to the high-gain construction. This in turn degrades the control quality and limits the closed-loop performance that can be achieved via ADRC. To address this problem, this paper investigates the implementation of noise suppressing ESOs in the context of PWR control for enhanced closed-loop performance. Design and implementation of noise suppressing ESOs are discussed in the subsequent sections.

IV. Cascade Extended State observer (CESO)

Cascade ESO [21], [22] operates by virtually splitting the total disturbance (f) into a predefined number of components $(f_i, i = \{1, ..., N\})$, each lying in a particular frequency range. These components are then estimated via N individual ESOs connected in cascade where the output of an ESO in each level acts as reference for the ESO in subsequent level. Cascade connection between subsequent ESOs results in additional filtering at each level and improves the sensitivity of final set of estimates towards high-frequency measurement noise. The ESO in each level is a Luenberger type observer constructed for the augmented state-space model given in (5) where the expression for i^{th} level ESO is given as follows:

$$\dot{\hat{\boldsymbol{z}}}_i = \boldsymbol{\mathcal{A}}\hat{\boldsymbol{z}}_i + b_0\boldsymbol{\mathcal{B}}u + \boldsymbol{\gamma_i}(y_{i-1} - \boldsymbol{C}\hat{\boldsymbol{z}}_{\boldsymbol{i}}) + \sum_{k=1}^{i-1}\boldsymbol{\Gamma}\hat{\boldsymbol{z}}_k, \tag{8}$$

where $\boldsymbol{\Gamma} = \begin{bmatrix} 0 & 0 & 0 \\ 0 & 0 & 1 \\ 0 & 0 & 0 \end{bmatrix}$, $\hat{\boldsymbol{z}}_i = [\hat{z}_{i,1}, \hat{z}_{i,2}, \hat{z}_{i,3}]^T$, $\boldsymbol{\gamma_i} = [\gamma_{1,i}\omega_{oi}, \gamma_{2,i}\omega_{oi}^2, \gamma_{3,i}\omega_{oi}^3]^T$, $y_i = \boldsymbol{C}\hat{\boldsymbol{z}}_{\boldsymbol{i}}, i = \{1, .., N\}, y_0 = y$. In order to reduce the number of tuning parameters in the ESOs, the observer gains are selected such that all the poles are placed at $-\omega_{oi}$ as per bandwidth parameterization approach highlighted in [29], which results in $\gamma_{1,i} = 3, \gamma_{2,i} = 3, \gamma_{3,i} = 1$, for third order ESOs used in the present study. Furthermore, the observer bandwidths for individual ESOs are selected as $\omega_{oi} = \omega_o a^{i-1},\ i = \{1, ..., N\}$ where $a > 1$ is a tuning parameter. The final set of estimates of the system states as well as total disturbance are obtained as

$$\hat{\boldsymbol{x}} = [\hat{x}_1, \hat{x}_2, \hat{x}_3]^T = \hat{\boldsymbol{z}}_N + \boldsymbol{E}\boldsymbol{E}^T\sum_{i=1}^{N-1}\hat{\boldsymbol{z}}_i, \tag{9}$$

where the state estimates of system states i.e. $\hat{x}_1, \hat{x}_2$ are obtained from the N^{th} level ESO while estimate of total disturbance is a sum of disturbance estimates obtained from each ESO.

We define a combined estimation error variable as $\boldsymbol{e_z} := [\boldsymbol{e_{z_1}^T}, \boldsymbol{e_{z_2}^T}, .., \boldsymbol{e_{z_N}^T}]^T$ where

$$\boldsymbol{e_{z_i}} := \boldsymbol{x} - \boldsymbol{\hat{x}_i},\ \boldsymbol{\hat{x}_i} = \boldsymbol{\hat{z}_i} + \boldsymbol{E}\boldsymbol{E}^T \sum_{j=1}^{i-1} \boldsymbol{\hat{z}_j},\ \boldsymbol{i} = \{1, .., N\}, \quad (10)$$

following the approach introduced in [22]. Considering a two level CESO which is used in the present study, the combined estimation error dynamics is given as

$$\boldsymbol{\dot{e}_z} = \boldsymbol{\mathcal{A}_z}\boldsymbol{e_z} + \boldsymbol{E_z}h - \boldsymbol{\gamma_z}\nu \quad (11)$$

where $\boldsymbol{\mathcal{A}_z} = \begin{bmatrix} \boldsymbol{\mathcal{A}} - \boldsymbol{\gamma_1 C} & \boldsymbol{0}_{3\times 3} \\ \boldsymbol{\gamma_2 C} - \boldsymbol{E}\boldsymbol{E}^T\boldsymbol{\gamma_1 C} & \boldsymbol{\mathcal{A}} - \boldsymbol{\gamma_2 C} \end{bmatrix}_{6\times 6}$, $\boldsymbol{E_z} = \begin{bmatrix} \boldsymbol{E} \\ \boldsymbol{E} \end{bmatrix}_{6\times 1}$, $\boldsymbol{\gamma_z} = \begin{bmatrix} \boldsymbol{\gamma_1} \\ \boldsymbol{E}\boldsymbol{E}^T\boldsymbol{\gamma_1} \end{bmatrix}_{6\times 1}$.

Since $\boldsymbol{\mathcal{A}_z}$ is Hurwitz by design, assuming that the derivative of total disturbance i.e. $\frac{df(\cdot)}{dt} = h$ and measurement noise ν are bounded in the sense that $|h| \leq \mu_1$ and $|\nu| \leq \mu_2$ where $\mu_1, \mu_2 > 0$, it can be shown that the actual estimation error vector defined as $\boldsymbol{e} := \boldsymbol{x} - \boldsymbol{\hat{x}} = [x_1 - \hat{x}_1, x_2 - \hat{x}, x_3 - \hat{x}_3]^T$ is bounded as

$$\lim_{t\to\infty} \|\boldsymbol{e(t)}\| \leq \kappa_1 a^2 \omega_o^{-1}\mu_1 + \kappa_2 a^2 \omega_o^2 \mu_2, \quad (12)$$

where $\kappa_1, \kappa_2 \geq 0$. The steady-state ultimate bound for $\|\boldsymbol{e}\|$ illustrates that the effect of disturbance on estimation error reduces upon increasing the value of ω_o, however, the obtained estimates become more sensitive to the effect of measurement noise. It is also evident that practical convergence of estimation error is only possible in the neighbourhood of origin and that the estimation error cannot be made arbitrarily small by selecting higher values of ω_o. It is to be noted that standard ESO used in conventional ADRC is a special case of CESO obtained for $N = 1$ and is therefore not discussed separately.

V. Low-power Higher-order Extended State Observer (LHESO)

In contrast to a standard ESO which assumes the disturbance to be constant [27], [30], a higher order ESO (HESO) incorporates a time polynomial type disturbance model into the augmented state-space form and is therefore more accurate in practical scenarios where disturbances are mostly time-varying. However, an HESO also suffers from the noise amplification problem that limits closed-loop performance in case of standard high-gain ESO. Furthermore, the numerical implementation issue [20] that is encountered in standard high-gain ESO gets aggravated in case of HESO as the gains escalate to $\mathcal{O}(\omega_o^{n+m})$ where m denotes the number of state augmentations. To mitigate these issues, the HESO is implemented via a low-power construction introduced in [31] which limits the magnitude of observer gain to $\mathcal{O}(\omega_o^2)$ and guarantees improved noise suppression in the estimates while simultaneously retaining all the good features of HESO such as asymptotic convergence of estimates in presence of disturbances that satisfy $\frac{d^m f(\cdot)}{dt^m} = 0$, when the effect of measurement noise is ignored.

In this study we consider a system having two state augmentations $(m = 2)$ which is given by

$$\begin{aligned} \boldsymbol{\dot{x}^+} &= \boldsymbol{\breve{\mathcal{A}}}\boldsymbol{x^+} + b_0\boldsymbol{\breve{\mathcal{B}}}u + \boldsymbol{\breve{E}}g \\ y &= \boldsymbol{\breve{C}}\boldsymbol{x^+} + \nu, \end{aligned} \quad (13)$$

where $\boldsymbol{x^+} = [\boldsymbol{x}^T x_4]^T$, $x_4 = \ddot{f} = g$, $\boldsymbol{\breve{\mathcal{A}}} = \begin{bmatrix} \boldsymbol{0} & \boldsymbol{I}_3 \\ 0 & \boldsymbol{0} \end{bmatrix}_{4\times 4}$, $\boldsymbol{\breve{\mathcal{B}}} = \begin{bmatrix} 0 & 1 & \boldsymbol{0} \end{bmatrix}_{1\times 4}^T$, $\boldsymbol{\breve{C}} = \begin{bmatrix} 1 & \boldsymbol{0} \end{bmatrix}_{1\times 4}$ and $\boldsymbol{\breve{E}} = \begin{bmatrix} \boldsymbol{0} & 1 \end{bmatrix}_{1\times 4}^T$. The resulting LHESO designed for (13) is expressed using the following set of equations:

$$\begin{aligned} \dot{\hat{x}}_i &= \hat{\bar{x}}_{i+1} + a_i b_0 u + \omega_o \beta_i (y_i - \hat{x}_i),\ i = \{1, .., m+1\} \\ \dot{\hat{\bar{x}}}_i &= \hat{\bar{x}}_{i+1} + a_i b_0 u + \omega_o^2 \bar{\beta}_i (y_{i-1} - \hat{x}_{i-1}),\ i = \{2, .., m\} \\ \dot{\hat{\bar{x}}}_{m+1} &= \omega_o^2 \bar{\beta}_{m+1} (y_m - \hat{x}_m), \end{aligned} \quad (14)$$

where $y_i = \begin{cases} \hat{\bar{x}}_i, & i = \{2, .., m\} \\ y, & i = 1 \end{cases}$, $a_i = \begin{cases} 1, & i = 2 \\ 0, & \text{otherwise.} \end{cases}$

Introducing estimation error vector as $\boldsymbol{e_\chi} := \boldsymbol{\chi} - \boldsymbol{\hat{\chi}}$ where $\boldsymbol{\hat{\chi}} := [\boldsymbol{\hat{\chi}_1^T}, \boldsymbol{\hat{\chi}_2^T}, \boldsymbol{\hat{\chi}_3^T}]^T$, $\boldsymbol{\hat{\chi}_i} := [\hat{x}_i,\ \hat{\bar{x}}_{i+1}]^T$, $\boldsymbol{\chi} = [x_1, x_2, x_2, x_3, x_3, x_4]^T$, we obtain error dynamics as

$$\boldsymbol{\dot{e}_\chi} = \boldsymbol{A_\chi}\boldsymbol{\chi} + \boldsymbol{\mathcal{H}}g - \boldsymbol{\mathcal{F}}\nu, \quad (15)$$

where $\boldsymbol{\mathcal{F}} = [l_1\omega_o, \bar{l}_1\omega_o^2, \boldsymbol{0}_{1\times 4}]^T$, $\boldsymbol{\mathcal{H}} = [\boldsymbol{0}_{1\times 5}, 1]^T$ while error matrix $\boldsymbol{A_\chi} = \boldsymbol{\Xi_3}$ can be obtained recursively in the following manner: $\boldsymbol{\Xi_1} = \boldsymbol{E_1}, \boldsymbol{\Xi_i} = \begin{bmatrix} \boldsymbol{\Xi_{i-1}} & \boldsymbol{\bar{N}_i} \\ \boldsymbol{\bar{Q}_i} & \boldsymbol{E_i} \end{bmatrix}, \boldsymbol{E_i} = \begin{bmatrix} -\beta_i\omega_o & 1 \\ -\bar{\beta}_i\omega_o^2 & 0 \end{bmatrix}, \boldsymbol{\bar{N}_i} = \begin{bmatrix} \boldsymbol{0_{2(i-2)\times 2}} \\ \boldsymbol{N} \end{bmatrix}, \boldsymbol{\bar{Q}_i} = \begin{bmatrix} \boldsymbol{0_{2\times 2(i-2)}} & \boldsymbol{Q_i} \end{bmatrix}, \boldsymbol{Q_i} = \begin{bmatrix} 0 & \beta_i\omega_o \\ 0 & \bar{\beta}_i\omega_o^2 \end{bmatrix}, \boldsymbol{N} = \begin{bmatrix} 0 & 0 \\ 0 & 1 \end{bmatrix}, i = \{2, 3\}$.

Assuming that $|g| \leq \mu_3$ where $\mu_3 \geq 0$, it can be shown that

$$\lim_{t\to\infty} \|\boldsymbol{e}(t)\| \leq \omega_o^{-1}\kappa_3\mu_3 + \omega_o^3\kappa_4\mu_2, \quad (16)$$

for $\kappa_3, \kappa_4 \geq 0$, where selection of ω_o presents a compromise similar to the case of CESO. The eigen values of $\boldsymbol{A_\chi}$ can be placed at $-\omega_o$ by selecting $\beta_i = 2,\ i = \{1, 2, 3\}$, $\bar{\beta}_1 = 3, \bar{\beta}_2 = 1$ and $\bar{\beta}_3 = 1/3$, based on the concept of bandwidth parameterization proposed in [29]. Such a selection also reduces the number of tuning parameters to unity and facilitates practical implementation. It is also worth noting that LHESO avoids the gain escalation problem which plagues high-gain observers (including ESO and CESO) and leads to numerical implementation complexity on fixed point digital signal processors by using gains that grow only up to ω_o^2 [20], [31]. Low-power construction of LHESO ensures that the relative degree between estimation error $e_i, i = \{1, 2, 3\}$ and measurement noise (ν) goes on increasing from unit to three as i increases. This results in superior noise suppression in the disturbance estimate $(\hat{x}_3)$ which is most affected by measurement noise among the required estimates.

VI. Simulation Results

Numerical simulation for the closed loop system is performed in Simulink/MATLAB environment using ode3 solver with a fixed sampling time of 0.1 ms. Dynamics of PWR is simulated using the nonlinear model expressed in (1) with the system parameters defined as $\Lambda = 10^{-4}s$, $\beta = 0.006019$, $\lambda = 0.15s^{-1}$, $G_r = 0.0145\delta k/k$, $\mu_f = 26.3MW \cdot s/^{\circ}C$, $T_{e0} = 290^{\circ}C$, $f_f = 0.92$, $P_0 = 2500MW$ [18]. The effect of measurement noise is included by passing a Band-limited Gaussian white noise having power 10^{-11}, through an 8^{th}-order Butterworth high-pass filter having pass band frequency of 200 rad/s. Performance of CESO and LHESO is compared to a conventional ESO to highlight the advantages of the two schemes. ESO, CESO and LHESO are implemented using the methods described in Section III, IV and V to obtain the estimates required for control law in (6),(7). The controller and observer parameters selected for the study are $\omega_c = 1$ rad/s, $\omega_o = \omega_{o2} = 40$ rad/s and $\omega_{o1} = 20$ rad/s. The controller as well as observer bandwidths of all three ESOs (ω_{o2} in case of CESO) are kept same for a fair comparison.

Performance of the closed-loop system is evaluated for reference tracking as well as disturbance attenuation under nominal and perturbed scenarios considering three different scenarios defined as follows: **S1-** Negative 10% step change in power reference applied at t=50 s. **S2-** Step change of -2°C in T_e applied at t=200 s. **S3-** Step decrease in reactivity by 0.0002 at t=290 s.

Under nominal condition, the plots for test scenarios S1-S3 are obtained in Fig. 1. For the reference tracking case in Fig. 1a, it can be observed that LHESO and CESO based closed-loop system settles to the new power reference much faster that ESO based approach with no overshoot in case of LESO and negligible overshoot for CESO. Furthermore, the control signal plot indicating velocity of the control rod (z_r) in Fig. 1b clearly shows in the zoomed-in view that LHESO based ADRC exhibits the best control quality (in terms of smoothness) and is least affected by the measurement noise present in the sensed data. Although CESO also suppresses the effect of measurement noise in control signal to a great extent (compared to conventional ESO), LHESO exhibits superior noise suppression due to its structural properties that result in increased relative degree [20]. For abrupt changes in T_e and ρ, LHESO and CESO based schemes yield significantly better regulation compared to ESO due to their enhance disturbance estimation capabilities.

Robustness of the designed schemes is investigated by introducing perturbation into the PWR parameters- G_r, β and λ, where each system parameter is perturbed by $\pm 20\%$ giving rise to eight different perturbed scenarios in total. Plots obtained for the perturbed case are given in Fig. 2 which indicate that the designed schemes are robust towards large perturbations in system parameters and are able to ensure system stability while tracking reference changes as well as under the effect of variations in T_e and reactivity.

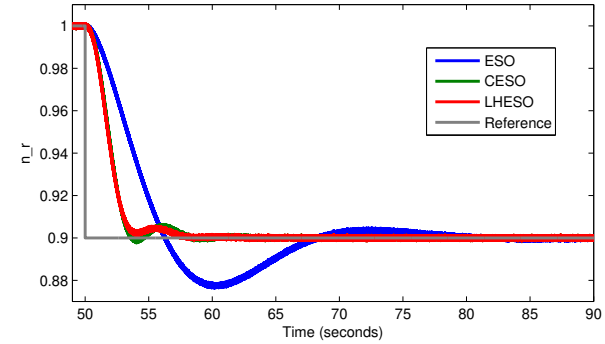

(a) **S1**

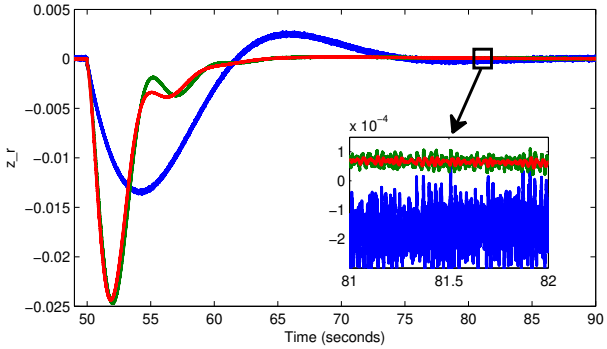

(b) **S1**

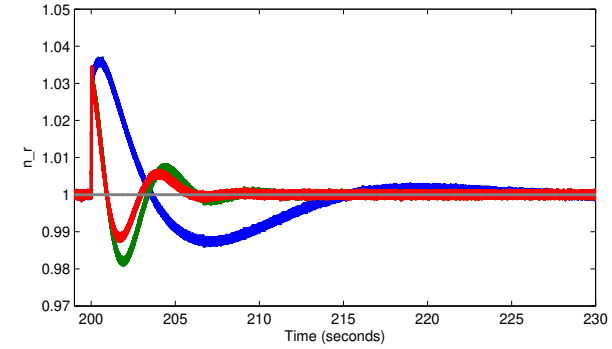

(c) **S2**

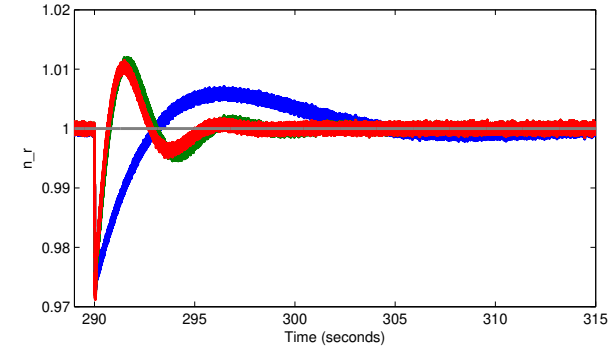

(d) **S3**

Fig. 1: Response to set-point changes and abrupt changes in T_e and ρ with measurement noise under nominal condition.

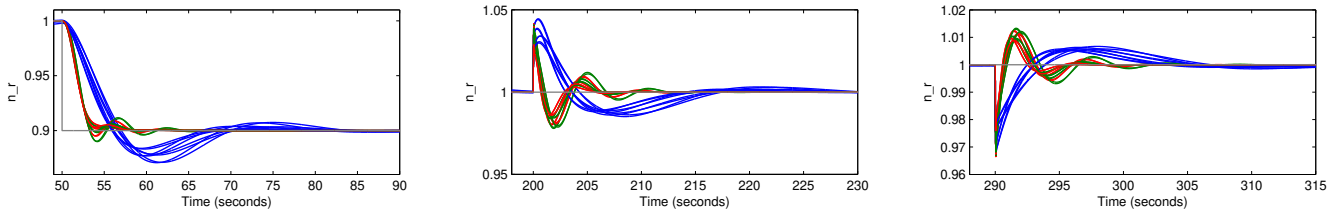

(a) **S1** (b) **S2** (c) **S3**

Fig. 2: Closed-loop system response under parametric perturbations without the effect of measurement noise (legend: red-LHESO, green-CESO, blue-ESO).

VII. Conclusion

This paper investigates the efficiency of recently proposed noise suppressing ESO's for control of PWR under practical operating conditions. Through extensive simulation studies, it is shown that the noise suppressing ESOs yield improved closed-loop performance compared to conventional ESO in terms of reference tracking as well as attenuation of disturbances. In addition to nominal operating condition, the closed-loop performance is evaluated under eight different combinations of parametric perturbations to evaluate the robustness of the three ESOs. Further improvements in performance as well as noise suppression can be obtained by combining the two structures and will be investigated in future works.

References

[1] L. Xia, J. Jiang, and J. C. Luxat, "Power distribution control of CANDU reactors based on modal representation of reactor kinetics," *Nuclear Engineering and Design*, vol. 278, pp. 323–332, 2014.

[2] G. Li and F. Zhao, "Flexibility control and simulation with multi-model and LQG/LTR design for PWR core load following operation," *Annals of Nuclear Energy*, vol. 56, pp. 179–188, 2013.

[3] J. Wan and P. Wang, "Lqg/ltr controller design based on improved sfacc for the pwr reactor power control system," *Nuclear Science and Engineering*, vol. 194, no. 6, pp. 433–446, 2020.

[4] G. Li and F. Zhao, "Load following control and global stability analysis for PWR core based on multi-model, LQG, IAGA and flexibility idea," *Progress in Nuclear Energy*, vol. 66, pp. 80–89, 2013.

[5] P. V. Surjagade, S. Shimjith, and A. Tiwari, "Second order integral sliding mode observer and controller for a nuclear reactor," *Nuclear Engineering and Technology*, vol. 52, no. 3, pp. 552–559, 2020.

[6] K. K. Abdulraheem and S. A. Korolev, "Robust optimal-integral sliding mode control for a pressurized water nuclear reactor in load following mode of operation," *Annals of Nuclear Energy*, vol. 158, p. 108288, 2021.

[7] V. Vajpayee *et al.*, "LQGI/LTR based robust control technique for a pressurized water nuclear power plant," *Annals of Nuclear Energy*, vol. 154, p. 108105, 2021.

[8] G. Wang, J. Wu, B. Zeng, Z. Xu, W. Wu, and X. Ma, "Design of a model predictive control method for load tracking in nuclear power plants," *Progress in Nuclear Energy*, vol. 101, pp. 260–269, 2017.

[9] X. Luan, J. Wang, Z. Yang, and J. Zhou, "Load-following control of nuclear reactors based on fuzzy input-output model," *Annals of Nuclear Energy*, vol. 151, p. 107857, 2021.

[10] D. A. Ejigu and X. Liu, "Gradient descent-particle swarm optimization based deep neural network predictive control of pressurized water reactor power," *Progress in Nuclear Energy*, vol. 145, p. 104108, 2022.

[11] G. Ansarifar, M. Nasrabadi, and R. Hassanvand, "Core power control of the fast nuclear reactors with estimation of the delayed neutron precursor density using sliding mode method," *Nuclear Engineering and Design*, vol. 296, pp. 1–8, 2016.

[12] H. Ahmed, I. Salgado, and H. Ríos, "Robust synchronization of master-slave chaotic systems using approximate model: An experimental study," *ISA transactions*, vol. 73, pp. 141–146, 2018.

[13] K. K. Abdulraheem, S. A. Korolev, and Z. Laidani, "A differentiator based second-order sliding-mode control of a pressurized water nuclear research reactor considering xenon concentration feedback," *Annals of Nuclear Energy*, vol. 156, p. 108193, 2021.

[14] K. K. Abdulraheem, A. O. Tolokonsky, and Z. Laidani, "Adaptive second-order sliding-mode control for a pressurized water nuclear reactor in load following operation with xenon oscillation suppression," *Nuclear Engineering and Design*, vol. 391, p. 111742, 2022.

[15] L. Ovalle, H. Ríos, and H. Ahmed, "Robust control for an active suspension system via continuous sliding-mode controllers," *Engineering Science and Technology, an International Journal*, vol. 28, p. 101026, 2022.

[16] A. Sun *et al.*, "Application of model free active disturbance rejection controller in nuclear reactor power control," *Progress in Nuclear Energy*, vol. 140, p. 103907, 2021.

[17] J. Hui, S. Ge, J. Ling, and J. Yuan, "Extended state observer-based adaptive dynamic sliding mode control for power level of nuclear power plant," *Annals of Nuclear Energy*, vol. 143, p. 107417, 2020.

[18] Y. Liu, J. Liu, and S. Zhou, "Linear active disturbance rejection control for pressurized water reactor power based on partial feedback linearization," *Annals of Nuclear Energy*, vol. 137, p. 107088, 2020.

[19] J. Hui and J. Yuan, "Load following control of a pressurized water reactor via finite-time super-twisting sliding mode and extended state observer techniques," *Energy*, vol. 241, p. 122836, 2022.

[20] S. Ahmad and A. Ali, "On active disturbance rejection control in presence of measurement noise," *IEEE Trans. Ind. Electron.*, pp. 1–1, 2021.

[21] K. Lakomy and R. Madonski, "Cascade extended state observer for active disturbance rejection control applications under measurement noise," *ISA Transactions*, vol. 109, pp. 1–10, 2021.

[22] K. Lakomy *et al.*, "Active disturbance rejection control design with suppression of sensor noise effects in application to DC-DC buck power converter," *IEEE Trans. Ind. Electron.*, vol. 69, no. 1, pp. 816–824, 2022.

[23] S. Shimjith, A. Tiwari, M. Naskar, and B. Bandyopadhyay, "Space–time kinetics modeling of advanced heavy water reactor for control studies," *Annals of Nuclear Energy*, vol. 37, no. 3, pp. 310–324, 2010.

[24] J. J. Duderstadt and L. J. Hamilton, *Nuclear reactor analysis*. Wiley, 1976.

[25] D. L. Hetrick, "Dynamics of nuclear reactors." 1971.

[26] J. Han, "From PID to active disturbance rejection control," *IEEE Transactions on Industrial Electronics*, vol. 56, no. 3, pp. 900–906, 2009.

[27] S. Ahmad and A. Ali, "Active disturbance rejection control of DC–DC boost converter: a review with modifications for improved performance," *IET Power Electronics*, vol. 12, no. 8, pp. 2095–2107, 2019.

[28] S. Ahmad and H. Ahmed, "Robust intrusion detection for resilience enhancement of industrial control systems: An extended state observer approach," in *2022 IEEE Texas Power and Energy Conference (TPEC)*.

[29] Z. Gao, "Scaling and bandwidth-parameterization based controller tuning," in *Proceedings of the American Control Conference (ACC)*, vol. 6, 2006, pp. 4989–4996.

[30] S. Ahmad and A. Ali, "Unified disturbance estimation based control and equivalence with IMC and PID: Case study on a DC–DC boost converter," *IEEE Trans. Ind. Electron.*, vol. 68, no. 6, pp. 5122–5132, 2021.

[31] D. Astolfi and L. Marconi, "A high-gain nonlinear observer with limited gain power," *IEEE Trans. Autom. Control*, vol. 60, no. 11, pp. 3059–3064, 2015.